DOI: 10.17344/acsi.2020.6503 *Acta Chim. Slov.* **2021,** *68,* 414–425
creative commons

Scientific paper

Effects of Tryptophan on the Polymorphic Transformation of Calcium Carbonate: Central Composite Design, Characterization, Kinetics, and Thermodynamics

Sevgi Polat,* Tuba Nur Ozalp-Sendur and Perviz Sayan

Department of Chemical Engineering, Faculty of Engineering, Marmara University, 34722, İstanbul, Turkey.

** Corresponding author: E-mail: sevgi.polat@marmara.edu.tr*
Phone: +90-2167773706, Fax: +90-2167773501

Received: 11-12-2020

Abstract

The objectives of this study were to: (i) determine the effects of tryptophan on the polymorphic phase transformation of $CaCO_3$, (ii) investigate the thermal degradation characteristics of $CaCO_3$ in terms of kinetics and thermodynamics using the Coats–Redfern method, and (iii) assess the influence of the experimental conditions on the vaterite composition of $CaCO_3$ using response surface methodology based on central composite design. First, the $CaCO_3$ crystals were prepared and analyzed using XRD, FTIR, SEM, BET, AFM, and zeta potential analysis. Based on the characterization results, the shape of the $CaCO_3$ crystals changed from smooth cubic calcite crystals to porous irregular spherical-like vaterite crystals with increasing tryptophan concentration. Meanwhile, the kinetic results showed that the thermal degradation of $CaCO_3$ followed the shrinkage geometrical spherical mechanism, R_3 and the average activation energy was 224.6 kJ/mol. According to the results of the experimental design, the tryptophan concentration was the most influential variable affecting the relative fraction of vaterite in the produced crystals. It can be concluded that tryptophan is important for better understanding and controlling the polymorph, size, and morphology of $CaCO_3$ crystals.

Keywords: Calcium carbonate; polymorphism; central composite design; kinetics; thermodynamics

1. Introduction

Calcium carbonate ($CaCO_3$) is one of the most abundant natural minerals, comprising approximately 5% of the Earth's crust. It has a wide range of potential applications in industry and biomineralization.[1,2] $CaCO_3$ takes various forms, including two hydrated crystal forms of ikaite ($CaCO_3 \cdot 6H_2O$) and monohydrate ($CaCO_3 \cdot H_2O$), an amorphous form, and three anhydrous crystalline polymorphs (calcite, aragonite, and vaterite).[3–5] The most abundant form of calcite in nature is as a stable thermodynamic phase in rhombohedral crystalline structure with cubic shaped.[6] Aragonite is metastable under ambient pressure and temperature and has a needle-like crystal shape with orthorhombic structure.[7] Vaterite is the thermodynamically least stable form of calcium carbonate and it has a spherical-like crystal shape with hexagonal structure.[8] All three of these forms of $CaCO_3$ can be prepared by carbonation process under appropriate conditions and the order of abundance from high to low is calcite, aragonite, and vaterite in nature.[9] The vaterite polymorph is the least abundant in nature but it of particular interest for use in biomedical applications owing to its high specific surface area, good water solubility and dispersion, and lower density compared to the other two crystal polymorphs.[10]

The properties of $CaCO_3$ are of particular importance in industrial applications, particularly the crystal structure, whiteness, chemical purity, specific surface area, particle size distribution, and morphology. Therefore, it is important to understand and have control of the different $CaCO_3$ polymorphs formed during crystallization, which has recently attracted growing research interest.[11] To the best of our knowledge, various physicochemical factors have been found to be responsible for the polymorphic phase transformation process of $CaCO_3$, such as temperature,[12] solvent type,[13] pH,[14] and initial supersaturation.[15] In addition, different additives, such as barium, strontium, and magnesium ions,[16,17] graphene oxide,[18] biocompatible polymeric additives such as bovine serum albumin and polydopamine,[19] selenic acid, arsenic acid, and silicic

acid,[20] and various types of amino acids,[21] have been shown to greatly affect the morphology and polymorphic composition of $CaCO_3$ and the performance of the resulting product. $CaCO_3$ polymorphism has been investigated previously but more work is needed to fully understand the factors that control the structure and morphology of $CaCO_3$ during its polymorphic transformation. Thus, in this study, we systematically investigated the effects tryptophan on the polymorphic phase transformation of $CaCO_3$. The structure, morphology, particle size, surface area, and surface charge of the polymorphs were analyzed in order to gain further understanding of the polymorphic transformation process for $CaCO_3$. Tryptophan was selected for this study because of the limited number of studies using tryptophan as an additive to investigate the

$CaCO_3$ polymorphism and the influence of this additive on $CaCO_3$ structural and morphological properties has not yet fully studied yet. We employed the Coats–Redfern method to estimate the activation energy of $CaCO_3$ crystals and to ascertain the thermal decomposition mechanism of $CaCO_3$. Moreover, experimental design was used to determine the effects of the process variables of temperature, stirring rate, and tryptophan concentration on the transformation of $CaCO_3$ polymorphs. The novelty of this work lies in the use of a suitable experimental design to investigate the variables that affect the polymorphic transformation of $CaCO_3$ and any possible interactions between the variables to determine the optimum conditions for maximizing the vaterite content. This in-depth investigation of the effects of the interactions between the process variables on $CaCO_3$ crystallization will provide very useful information for industry and researchers.

2. Experimental

2. 1. Materials

Analytical-grade calcium chloride dihydrate ($CaCl_2 \cdot 2H_2O$), sodium carbonate (Na_2CO_3), and tryptophan ($C_{11}H_{12}N_2O_2$) were purchased from Merck. All solutions were prepared using distilled water.

2. 2. Experimental Method

$CaCO_3$ was prepared by the reaction between $CaCl_2 \cdot 2H_2O$ and Na_2CO_3 in a glass crystallizer with an active volume of 1.0 L. At the beginning of the experiment, 0.2 M calcium chloride solution (0.4 L) was placed into the crystallizer. After thermal equilibrium was reached, a 0.2 M sodium carbonate solution (0.4 L) was fed into the crystallizer at a rate of 4 mL/min using a peristaltic pump. The suspension in the crystallizer was stirred at a rate of 500 rpm. During the polymorphic transformation process, the pH of the solution was continuously monitored via a pH probe inserted into the crystallizer and maintained at pH 8.5 by the addition of dilute sodium hydroxide or hydrochloric acid solution by an automatic pH control system. The suspension temperature was maintained at a 30 ± 0.1 °C. At 30 and 100 min, 20-mL aliquots of the suspension were removed and used for crystal structure and morphology analysis.

The effect of tryptophan and its concentrations on the polymorphic transformation of $CaCO_3$ was investigated in this study. The specific amount of the tryptophan (corresponding to 50 ppm and 100 ppm) was added into the crystallizer at the beginning of the experiment. The product obtained was collected, filtered by using 0.45 μm membrane filters, washed with distilled water, and finally dried at room temperature. The prepared samples were treated prior to further analysis.

2. 3. Analysis

The precipitated $CaCO_3$ were analyzed for structure, functional group, crystal size, morphology, surface charge and thermal characteristics. Firstly, X-ray diffraction (XRD, Bruker D2 Phaser Table-top Diffractometer) was used to determine the phase structures of the $CaCO_3$ polymorphs and scanned in the range of 10 to 70° with a scan rate of 3°/min. The calcite and vaterite polymorphs in the $CaCO_3$ were quantitatively determined using the Rietveld refinement method. Meanwhile, the polymorphic transformation was monitored by Fourier transform infrared spectroscopy (FTIR; Shimadzu IR Affinity-1) equipped with Attenuated Total Reflectance (ATR) accessories. The spectra were recorded with scanning range from 600 to 2000 cm^{-1} at room temperature in transmission mode with a resolution of 4 cm^{-1}. The crystal morphologies of the $CaCO_3$ were investigated by scanning electron microscopy (SEM/EDX; Zeiss EVO LS w10) and the particle size distributions were measured with a Malvern Mastersizer 2000 instrument. Zeta potential measurements were conducted using a Malvern Zeta Sizer Nano Series Nano-ZS. The thermal behavior of the $CaCO_3$ precipitated in pure and tryptophan media was determined using a Setaram LABSYS Evo thermogravimetric analyzer in a nitrogen atmosphere between 50 °C and 950 °C with a heating rate of 10 °C/min. Using the obtained data, the thermal decomposition kinetics for the $CaCO_3$ crystals precipitated in pure media were investigated and the kinetic parameters were calculated.

2. 4. Coats–Redfern Method

The Coats–Redfern[22] model-fitting method is widely used for estimating the pre-exponential factor and activation energy to predict the order of a reaction. The basic equation for the Coats–Redfern method is as follows:

$$\ln\left[\frac{g(\alpha)}{T^2}\right] = \ln\left[\frac{AR}{\beta E_a}\left(1-\frac{2RT}{E_a}\right)\right] - \frac{E_a}{RT} \quad (1)$$

where β is the heating rate, R is the ideal gas constant (8.314 J/mol K), and $g(\alpha)$ is a kinetic function of different

Table 1. Reaction mechanisms and symbols with their f(α) and g(α).

Mechanisms	Symbol	f(α)	g(α)
Reaction order			
First-order	F_1	$(1-\alpha)$	$-\ln(1-\alpha)$
Second-order	F_2	$(1-\alpha)^2$	$(1-\alpha)^{-1}-1$
One and half order	$F_{1.5}$	$(1-\alpha)^{3/2}$	$2[(1-\alpha)^{-1/2}-1]$
Diffusion phenomena			
Parabolic Law	D_1	0.5α	α^2
Valensi equation	D_2	$[-\ln(1-\alpha)]^{-1}$	$\alpha+(1-\alpha)\ln(1-\alpha)$
Phase interfacial reaction			
Shrinkage geometrical column	R_2	$2(1-\alpha)^{1/2}$	$1-(1-\alpha)^{1/2}$
Shrinkage geometrical spherical	R_3	$3(1-\alpha)^{2/3}$	$1-(1-\alpha)^{1/3}$
Exponential nucleation			
Power law, n = 1/2	P_2	$2\alpha^{1/2}$	$\alpha^{1/2}$
Power law, n = 1/3	P_3	$3\alpha^{2/3}$	$\alpha^{1/3}$
Nucleation and growth			
Avrami-Erofeev two dimensional	A_2	$2(1-\alpha)[-\ln(1-\alpha)]^{1/2}$	$[-\ln(1-\alpha)]^{1/2}$
Avrami-Erofeev three dimensional	A_3	$3(1-\alpha)[-\ln(1-\alpha)]^{1/3}$	$[-\ln(1-\alpha)]^{1/3}$

reaction mechanisms that is obtained from integration of *f(α)*. The activation energy *(E_a)* can be determined by plotting a graph of 1/T versus ln [g(α)/T^2] and determining the slope of the straight line of best fit. The intercept of the line gives the pre-exponential factor *(A)* and g(α) varies depending on the developed model and reaction mechanism. Most solid-state degradation reactions fall into one of five main categories, as detailed in Table 1.[23,24]

2. 5. Thermodynamic Analysis

The thermodynamic parameters of the $CaCO_3$ crystals, including change in enthalpy (Δ*H*), change in Gibbs free energy (Δ*G*), and change in entropy (Δ*S*), were calculated based on kinetic data from the following equations[25]

$$\Delta H = E_\alpha - RT \tag{2}$$

$$\Delta G = E_\alpha + RT_{peak} \ln\left(\frac{K_B T_{peak}}{hA}\right) \tag{3}$$

$$\Delta S = \frac{\Delta H - T\Delta G}{T_{peak}} \tag{4}$$

Where T_{peak} is the peak temperature of DTG curve, K_B is the Boltzmann constant, and *h* is the Planck constant.

3. Results and Discussion

3. 1. XRD Analysis

The XRD patterns of the samples at 30 and 100 min during the polymorphic transformation process from calcite to vaterite in the presence of 50 ppm and 100 ppm tryptophan are shown in Figure 1. The XRD results indicate that the $CaCO_3$ crystals precipitated in pure media were only in calcite form (JCPDS: 05-0586) and no intermediate phase was produced in pure media. The main peaks observed at 2θ of 23.1°, 29.4°, 35.9°, and 39.3° are diffraction peaks corresponding to the calcite crystals lat-

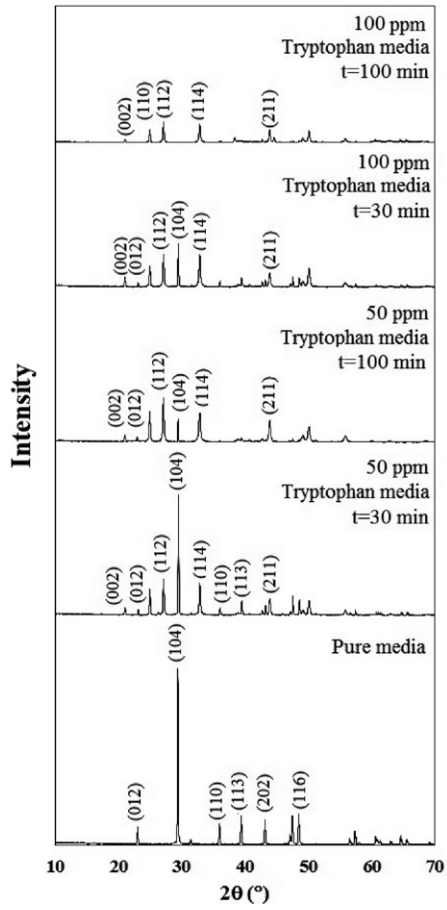

Figure 1. XRD results for $CaCO_3$ crystals precipitated in pure media and media supplemented with 50 and 100 ppm tryptophan.

tice planes of (012), (104), (110), and (113), respectively. When 50 ppm tryptophan was added to media, the resulting crystals included both calcite and vaterite forms together. The solid sample taken at 30 min showed the appearance of new peaks at 2θ = 21.0°, 24.9°, 27.1°, 32.7°, and 50.1°, which were assigned to the (002), (110), (112), (114), and (118) lattice faces of vaterite, respectively (JCPDS: 33-0268). Rietveld refinement quantitative analysis determined the calcite and vaterite contents to be 74.84% and 25.16%, respectively, for the 30-min sample obtained from media supplemented with 50 ppm tryptophan. As the transformation process progressed further, more of the vaterite form (41.20%) was found in the crystal sample. The intensity of the characteristic diffraction peaks of vaterite was obviously increased and more of the vaterite polymorph was obtained with time.

When the tryptophan concentration was 100 ppm, both calcite and vaterite diffraction peaks were observed in the solid sample obtained at 30 min during the polymorphic transformation process and the mass fractions of calcite and vaterite were calculated to be 61.26% and 38.74%, respectively. The results of Rietveld refinement quantitative analysis showed that the vaterite content increased with the increasing tryptophan concentration. In the sample obtained at 100 min, the characteristic diffraction peaks of calcite had completely disappeared, showing that all the calcite crystals were completely transformed into the vaterite form. The XRD results indicated that tryptophan influenced the crystal structure of calcium carbonate.

3. 2. FTIR Analysis

The FTIR spectra for $CaCO_3$ crystals precipitated with and without tryptophan at 30 and 100 min during the polymorphic phase transformation are presented in Figure 2.

The calcite and vaterite absorption peaks are at different positions in the FTIR spectra. The absorption peak at 712 cm^{-1} is the characteristic peak of calcite, while the absorption peaks at 1085 cm^{-1} and 746 cm^{-1} correspond to vaterite.[26] The FTIR spectrum for the $CaCO_3$ crystals precipitated in pure media displayed the characteristic band of the calcite polymorph at 713 cm^{-1}. At t = 30 min, the two main characteristic peaks of vaterite were identified for the $CaCO_3$ crystals precipitated in the presence of 50 ppm tryptophan. Meanwhile, the intensity of the absorption peak at 713 cm^{-1} became obviously weaker. As the transformation progressed further, the intensity of the characteristic FTIR peaks of vaterite, especially that at 746 cm^{-1}, obviously increased while the intensity of the absorption peak at 713 cm^{-1} decreased. These FTIR results show the change of the crystal polymorphs from calcite only to a mixture of vaterite and calcite with a higher proportion of vaterite than calcite. With the higher tryptophan concentration, the intensity of the vaterite peak became stronger, while the corresponding peak of calcite became weaker. For the solid sample obtained at 100 min,

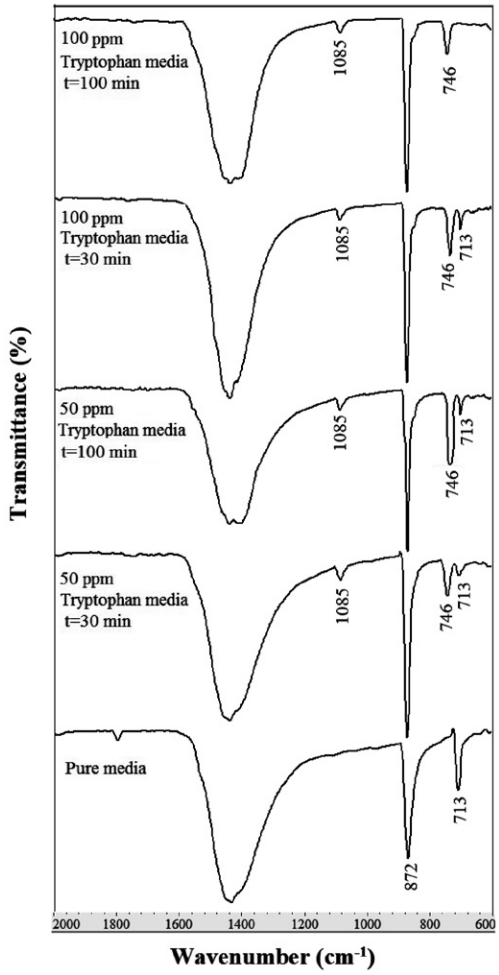

Figure 2. FTIR results for $CaCO_3$ crystals precipitated in pure media and media supplemented with 50 and 100 ppm tryptophan.

the absorption peak at 713 cm^{-1} had completely disappeared in the FTIR spectrum and the sample mainly consisting of the vaterite polymorph and water, which was consistent with the XRD results.

3. 3. SEM Analysis

The SEM image in Figure 3a shows that the surface of the $CaCO_3$ crystals precipitated in pure media was smooth and non-porous and the crystals were composed of regular cubic-shaped particles with nearly uniform size, which was in agreement with the results of previous studies.[27,28] Energy dispersive X-ray (EDX) spectroscopy was applied to determine the elemental composition of the $CaCO_3$ crystals. The EDX analysis showed a surface composition of Ca 40.12 wt%, C 11.97 wt%, and O 47.91 wt% for the crystals precipitated in pure media. The elemental content in $CaCO_3$ was thus consistent with the theoretical values. The average particle size and BET surface area of the $CaCO_3$ were 32 μm and 0.70 m^2/g, respectively. Based on the previous studies,[29–32] $CaCO_3$ crystals precipitated without additive were generally characterized by small

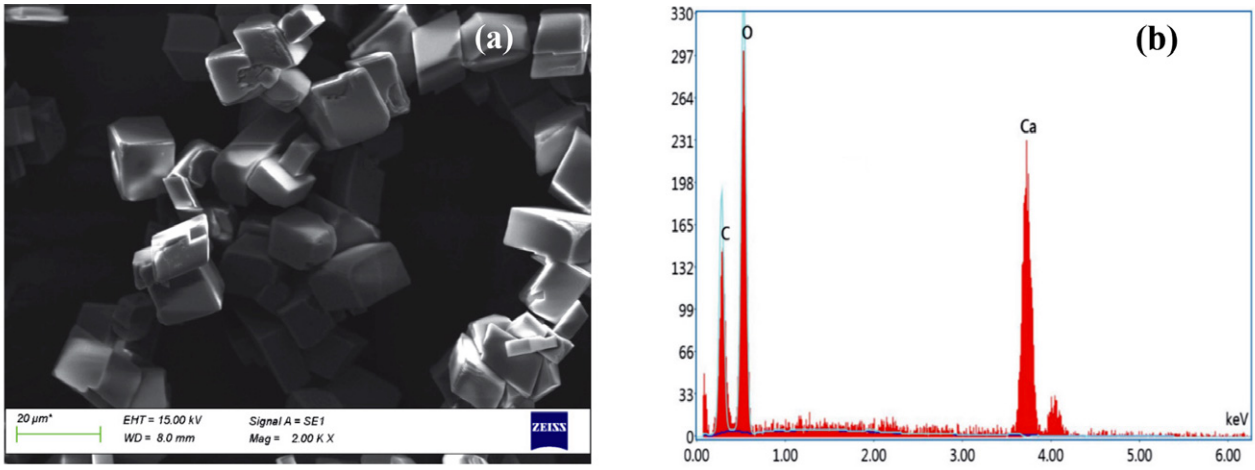

Figure 3. a) SEM and b) EDX results of $CaCO_3$ crystals precipitated in pure media.

surface areas, below 1 m^2/g, which was consistent with our result.

The SEM images of the $CaCO_3$ crystals precipitated in the presence 50 and 100 ppm tryptophan at different time points are presented in Figure 4.

At t = 30 min, in addition to cubic-shaped calcite crystals with an irregular surface, some small spherical-shaped plate-like vaterite crystals were observed for the 50 ppm additive media. That is, calcite and vaterite crystals were seen together, which was consistent with the XRD and FTIR results. With the increase of the transformation time to 100 min, the amount of cubic-shaped crystals decreased, surface deformations occurred on the calcite crystals, and some of the calcite was transformed to vaterite form. A similar outcome was also observed for crystals precipitated with 100 ppm tryptophan at 30 min. In addition to cubic calcite crystals, the sample also consisted of elliptical, intertwined, and compact agglomerates.

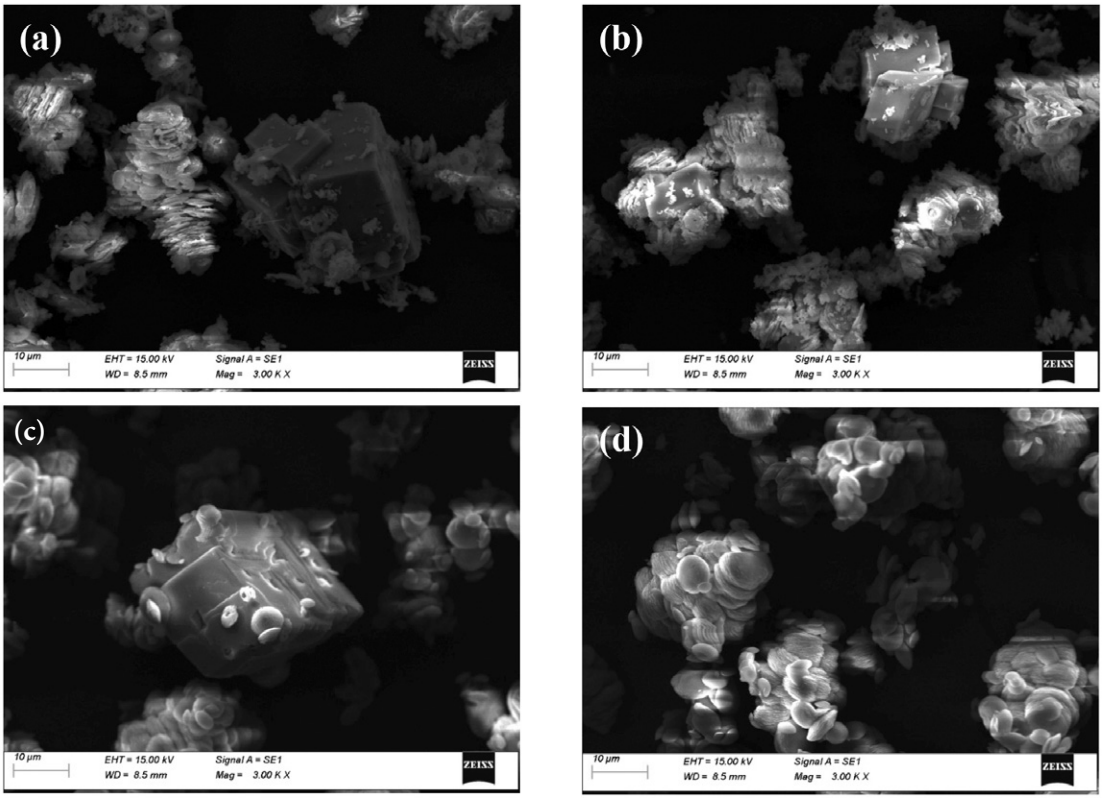

Figure 4. SEM images for $CaCO_3$ crystals precipitated with 50 ppm tryptophan at t = 30 min (a) and at t = 100 min (b) and with 100 ppm tryptophan at t = 30 min (c) and at t = 100 min (d).

These agglomerates took a spherical form owing to the effects of the hydrodynamic conditions of the media. At t = 30 min, both calcite and vaterite crystals were obtained. As the transformation process progressed, the cubic-shaped crystals disappeared completely and transformed into spherical-like vaterite crystals with an irregular crystal surface. With the completion of the transformation process, the obtained crystals had a spherical and ellipsoidal form, indicating that the calcite polymorph was completely converted into vaterite, which was also confirmed by the XRD and FTIR results. Meanwhile, the particle size and BET surface area of the samples precipitated in media supplemented with tryptophan were changed compared to the pure media due to the surface adsorption of the additive. The average particle sizes and BET surface areas of the samples precipitated in the presence of 50 and 100 ppm tryptophan were 26 μm and 3.8 m^2/g and 19 μm and 6.4 m^2/g, respectively. A higher additive concentration led to a decrease in the particle size and an increase in the specific surface area of the $CaCO_3$. Thus, more porous and rougher crystals with smaller sizes were produced in the presence of tryptophan.

To gain more insight into the effects of tryptophan on the topography of $CaCO_3$, AFM analysis was performed and 3D micrographs for the crystals precipitated with and without tryptophan are shown in Figure 5. The surface topography of the $CaCO_3$ crystals precipitated in pure media was flat and smooth with a maximum thickness of 31.17 nm. Compared to the crystals obtained in pure media, some ridges, defects, and irregularity occurred on the surface of $CaCO_3$ crystals precipitated in 100 ppm tryptophan media and the thickness increased to 117.45 nm. These changes led to increased surface roughness, confirming the results obtained from the SEM images.

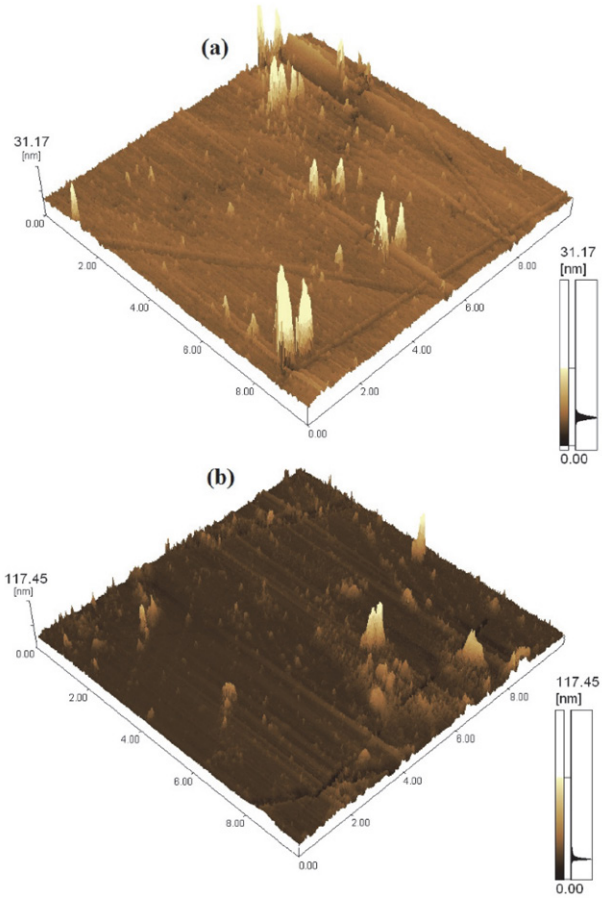

Figure 5. 3D micrographs for the crystals precipitated without (a) and with 100 ppm tryptophan (b).

3. 4. Zeta Potential Analysis

The zeta potential of the $CaCO_3$ crystals precipitated with and without tryptophan in the media was investigated to determine the surface charge and stability of a suspension of particles. The $CaCO_3$ crystals prepared in pure media had a zeta potential of –8.1 ± 2.1 mV. Similar to pure media, the zeta potential of $CaCO_3$ crystals precipitated in additive media had a negative value. The zeta potential values at 50 ppm were –15.7 ± 1.0 mV, –17.4 ± 1.8 mV for t = 30 and 100 mins, respectively. As the tryptophan concentration increased, the zeta potential value of the $CaCO_3$ crystals showed a clear increase. The zeta potential values reached –19.2 ± 1.3 mV and –25.7 ± 2.2 mV at 100 ppm for t = 30 and 100 mins, respectively, which obviously illustrated that the electrical surface charge of the $CaCO_3$ crystals was more negative at a higher tryptophan concentration. This change in the zeta potential suggests that some tryptophan was adsorbed on the surface of $CaCO_3$ crystals. In addition, the variations in zeta potentials in the additive media were associated with the changing agglomeration tendency of the crystals, which is supported with the results of SEM analysis.

3. 5. Filtration Analysis

Filtration is an important parameter for controlling the precipitation of $CaCO_3$ since it affects both the properties of the crystalline products and process efficiency which is important from an economic point of view. In order to determine how tryptophan influences the filtration characteristics of $CaCO_3$, the average specific cake resistance and the average cake porosity of the crystals were analyzed based on Darcy's Law under 700 mbar constant pressure. The average specific cake resistance and the average cake porosity of the crystals precipitated in pure media were 1.03×10^{12} m/kg and 0.548, respectively. The filtration characteristics of the $CaCO_3$ are significantly changed by the addition of tryptophan to the media. Average specific cake resistances of 9.65×10^{11} m/kg and 4.24×10^{11} m/kg were obtained at the end of the polymorphic transformation process with tryptophan at 50 and 100 ppm, respectively. A higher concentration of tryptophan led to a lower specific cake resistance. Meanwhile, the average cake porosity increased from 0.658 to 0.712 as the tryptophan concentration increased from 50 to 100 ppm. This can be explained

by the changes to the particle size, morphology, and polymorphic form, which have the greatest effect on these filtration characteristics. Fairly large differences in the sizes and shapes of the $CaCO_3$ crystals that were formed in the presence of tryptophan could be seen in the SEM images; these changes had a direct impact on the filtration properties. Therefore, appropriately increasing the tryptophan concentration could be advantageous for increasing the filtration rate and improving the filtration characteristics.

3. 6. Thermogravimetric Analysis

The thermogravimetric (TG) and differential thermogravimetric (DTG) curves for the crystals precipitated in pure media and with 100 ppm tryptophan are presented in Figure 6. Considering the thermal degradation characteristics of $CaCO_3$ crystals precipitated in pure media, a single DTG peak was observed, which showed that degradation occurred at a single stage, corresponding to the transformation of calcium carbonate to calcium oxide.[33,34] Thermal degradation occurred between 630 °C and 830 °C and the residual mass was 55.6 wt%, agreeing with the theoretical value. The weight loss from the $CaCO_3$ crystals precipitated in tryptophan media was 45.2 wt%. The higher weight loss suggests that tryptophan had been adsorbed onto and interacted with the surface of the $CaCO_3$ crystals. The addition of tryptophan had a slight effect on the temperature of the decomposition peak during the thermal decomposition of $CaCO_3$. While the maximum peak temperature was 809 °C for pure media, the value observed for the additive media was determined to be 821°C. Thus, adding tryptophan to the crystallization media shifted the decomposition peak to higher temperature.

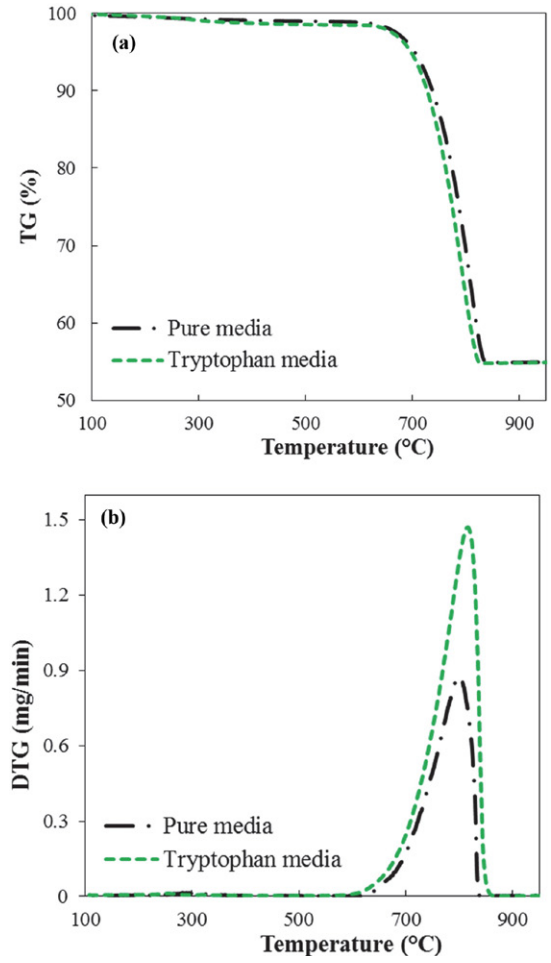

Figure 6. a) TG and b) DTG curves of $CaCO_3$ crystals precipitated in pure media and with 100 ppm tryptophan.

3. 7. Kinetic and Thermodynamic Analysis

In this study, the Coats–Redfern method was used to predict kinetic parameters such as activation energy and pre-exponential factor. The minimum energy required to initiate a reaction, known as the activation energy, can be determined by kinetic analysis. As shown in Table 2, the activation energies were between 56.6 and 442.6 kJ/mol, which was consistent with the results of previous studies.[35,36] The pre-exponential factors were in the range of 3.08×10^1 to 6.11×10^{20} min^{-1}, in good agreement with the literature.[36]

Linear adjustment using the different reaction mechanisms as shown in Table 1 was applied to estimate the reaction mechanism for the thermal degradation of $CaCO_3$.

Table 2. Kinetic calculation results for thermal decomposition of $CaCO_3$ using the Coats–Redfern method.

Symbol	E_a (kJ/mol)	A (min^{-1})	R^2	ΔH (kJ/mol)	ΔG (kJ/mol)	ΔS (J/mol · K)
F_1	242.8	1.86×10^{11}	0.9891	233.8	286.4	–48.6
F_2	281.0	3.09×10^{13}	0.9813	272.0	278.6	–6.09
$F_{1.5}$	257.8	1.53×10^{12}	0.9908	248.8	282.4	–31.1
D_1	423.1	9.98×101^9	0.9772	414.1	285.8	118.5
D_2	442.6	6.11×10^{20}	0.9842	433.6	289.0	133.6
R_2	218.9	4.87×10^9	0.9865	209.9	295.3	–78.9
R_3	**224.6**	**6.88×10^9**	**0.9954**	**215.6**	**297.9**	**–76.0**
P_2	93.3	4.27×10^6	0.9698	84.3	233.0	–137.4
P_3	56.6	3.08×10^1	0.9630	47.6	302.9	–235.8
A_2	110.1	2.93×10^4	0.9892	101.2	294.7	–178.8
A_3	69.8	1.98×10^2	0.9850	60.8	299.4	–220.4

It was found from Table 2 that the thermal degradation of $CaCO_3$ predicted by the geometric spherical shrinkage mechanism (the R_3 type model) fitted the experimental data best, which was consistent with previous research.[35,36] The regression coefficients ranged between 0.9630 and 0.9954 depending on the applied kinetic model. The R_3 type model presented the highest accuracy (R^2 = 0.9954) of the 11 models studied.

The thermodynamic parameters of enthalpy (ΔH), entropy (ΔS), and Gibbs free energy (ΔG) for the thermal decomposition of $CaCO_3$ were calculated using different reaction mechanism models. According to the thermodynamic results presented in Table 2, the enthalpy change for the thermal decomposition of $CaCO_3$ was between 47.6 and 433.6 kJ/mol depending on the model used. Diffusion models D1 and D2 gave higher ΔH values that the other models tested, including the reaction, interfacial, exponential, nucleation, and growth models. The positive values of ΔH obtained for the crystals confirmed that the main decomposition process was endothermic in nature. The entropy changes for the crystals were in the range of −235.8 to 133.6 J/mol K. All of the tested models showed negative ΔS values except for D1 and D2. The negative ΔS values show that the disorder of the products obtained through bond dissociation was lower than that of the initial reactants. These negative values suggest that the disintegration product from the activated state has a more well-organized structure than before the thermal disintegration and that the reactions in the activated state proceed more gently than anticipated. The Gibbs free energy change was calculated to be between 233.0 and 302.9 kJ/mol. A positive value of ΔG indicates that a reaction is unfavorable and thus energy needs to be supplied for the reaction to occur.

3. 8. Experiment Design Results

Response surface methodology (RSM) is a multivariate statistical technique that is used to optimize process variables and their responses by exploring the relationship between independent process variables and their observed responses. Box–Behnken design, central composite design (CCD), and three-level factorial design are examples of experimental design techniques, with CCD being the most effective and popular method. In this study, Design Expert software version 10 (Stat-Ease, Minneapolis, USA) was used for the experimental design using CCD.[37] We conducted 17 experiments with three center points using three variables of temperature (A), stirring rate (B), and tryptophan concentration (C), and the vaterite content was chosen as the response. Meanwhile, CCD with three factors and five levels was also applied to determine the correlation between the combined effects of individual variables. Tables 3 and 4 show the range and levels, respectively, of the investigated variables and their responses for all 17 optimized test experimental runs.

Thus, based on these results, the model equation for the vaterite content as a function of the process variables is:

Table 3. Experimental variables and their levels in central composite design matrix.

Parameters	Factors	Levels				
		−2	**−1**	**0**	**+1**	**+2**
Temperature (°C)	A	20	25	30	35	40
Stirring rate (rpm)	B	400	450	500	550	600
Tryptophan concentration (ppm)	C	0	25	50	75	100

Table 4. Central composite design matrix and results.

Run	Actual level of factors			Coded level of factors			Response
	Temperature (°C)	Stirring rate (rpm) (ppm)	Concentration	A	B	C	Vaterite composition (%)
1	25	450	25	−1	−1	−1	19.2
2	35	450	25	+1	−1	−1	27.2
3	25	550	25	−1	+1	−1	25.4
4	35	550	25	+1	+1	−1	31.6
5	25	450	75	−1	−1	+1	60.6
6	35	450	75	+1	−1	+1	70.3
7	25	550	75	−1	+1	+1	64.4
8	35	550	75	+1	+1	+1	75.9
9	20	500	50	−2	0	0	34.7
10	40	500	50	+2	0	0	44.4
11	30	400	50	0	−2	0	40.6
12	30	600	50	0	+2	0	51.8
13	30	500	0	0	0	−2	0
14	30	500	100	0	0	+2	100
15	30	500	50	0	0	0	41.8
16	30	500	50	0	0	0	42.4
17	30	500	50	0	0	0	41.0

$$Y = 42.59 + 3.42A + 2.65B + 22.99C + 0.87AC - \\ - 0.15BC - 0.44A^2 + 1.22B^2 + 2.17C^2 \quad (5)$$

The lowest vaterite composition (19.2%) was obtained at 25 °C, 450 rpm, and 50 ppm tryptophan concentration (apart from the sample obtained in pure media at 30 °C and 500 rpm).

The model and factor significances with respect to vaterite content were examined by variance analysis (ANOVA) of the F test and p-values. The results are shown in Table 5. The obtained values of F and p suggest that the experimental values are significant and thus acceptable. The ANOVA results showed a large F of 63.59 and a small *p*-value << 0.0001, which verified that the model fit was statistically significant. The obtained correlation coefficient (R^2) of 0.9879 showed that there was good correlation between the measured and predicted responses and confirmed that the model was suitable for the experimental data. The CCD analysis shows that the three independent process variables played an important role in determining the amounts of the $CaCO_3$ polymorphs formed since its p-value was <0.05 and had positive coefficients. Increasing the temperature, stirring rate, and tryptophan concentration increased the amount of vaterite formed and they were thus significant and favorable factors. However, the strength and significance of the effect varied for each parameter. The p-value of <0.0001 for tryptophan concentration shows that it is the most important variable to control. However, the interaction of tryptophan concentration with other parameters had a less significant effect. Thus, this establishes tryptophan concentration as the most influential parameter during the polymorphic transformation of $CaCO_3$.

The effects of the independent variables and their interactions are presented in the three-dimensional (3D) response surface plots and contour plots in Figure 7.

According to the results, the 3D surface plots are flat with the slope being related to linear terms of the variables. As shown in Figure 7, when more than one factor is changed at a time, different effects on the response are observed. The highest vaterite content was obtained with the highest additive concentration, temperature, and stirring rate. In comparison with temperature and stirring rate, tryptophan concentration had the most significant effect on the amount of vaterite produced.

4. Conclusions

In this work, the precipitation of $CaCO_3$ was investigated in the presence of different concentrations of tryptophan. XRD results showed that using 50 ppm tryptophan as an additive increased the vaterite content by 50.0% compared to pure media. In parallel with the XRD results, FTIR analysis demonstrated that the polymorphic transformation from calcite to vaterite was completely achieved in the presence of 100 ppm tryptophan. SEM images illustrated that tryptophan contributed to the formation of spherical vaterite crystals with a small crystal size. BET analysis showed that the addition of 100 ppm tryptophan increased the BET specific surface area from 0.7 to 6.4 m^2/g. Zeta potential analysis suggested that the tryptophan tended to adsorb on the crystal surface. Filtration analysis showed that a higher tryptophan concentration led to a higher average cake porosity and a lower specific cake resistance. In this study, the thermal degradation kinetics of $CaCO_3$ were also explored using the Coats–Redfern method. The thermal decomposition kinetics predicted by the R_3 type model showed the best agreement with the experimental data out of the 11 tested models with high accuracy (R^2 = 0.9954). Additionally, this study also provided a thermodynamic analysis of $CaCO_3$ crystals. Based on the R_3 type model, the ΔH, ΔG, and ΔS were calculated to be 215.6 kJ/mol, 297.9 kJ/mol, and −76.0 J/mol K, respectively. CCD with RSM was applied successfully to determine how temperature, stirring rate, and tryptophan

Table 5. ANOVA results of the quadratic model for vaterite content.

Source	Sum of Squares	df	Mean Square	F-Value	p-value Prob > F
Model	8904.63	9	989.40	63.59	< 0.0001
A-Temperature	187.69	1	187.69	12.06	0.0104
B-Stirring rate	112.36	1	112.36	7.22	0.0312
C- Tryptophan concentration	8454.80	1	8454.80	543.43	< 0.0001
AB	0.000	1	0.000	0.000	1.0000
AC	6.13	1	6.13	0.39	0.5503
BC	0.18	1	0.18	0.012	0.9174
A^2	3.73	1	3.73	0.24	0.6391
B^2	28.99	1	28.99	1.86	0.2145
C^2	91.49	1	91.49	5.88	0.0458
Residual	108.91	7	15.56		
Lack of Fit	107.92	5	21.58	43.75	0.0225
R^2	0.9879				

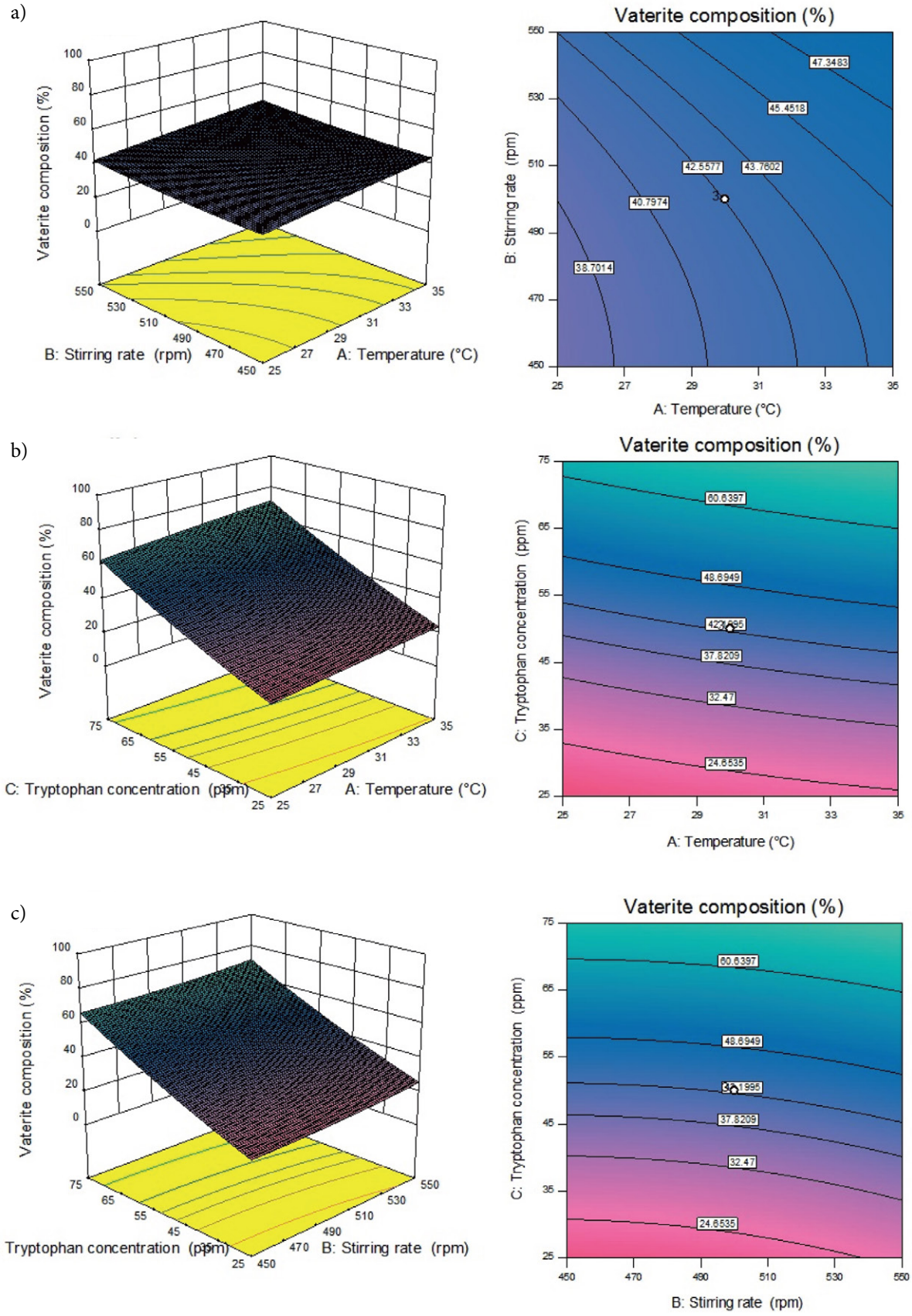

Figure 7. 3D-surface and contour plots showing the effects of (a) temperature and stirring rate; (b) temperature and tryptophan concentration; and (c) stirring rate and tryptophan concentration on the vaterite composition.

concentration influenced the $CaCO_3$ polymorphic phase transformation in terms of the amount of vaterite produced. The experimental design results showed that among the investigated factors, additive concentration had the greatest effect on the vaterite content. The detailed information about the characterization, kinetics, thermodynamics, and optimization of $CaCO_3$ crystallization obtained in this work will provide a reference for the polymorphic transformation of calcium carbonate for scientific and industrial purposes.

Acknowledgements

This work was supported by Marmara University Scientific Research Projects Commission under the funding FYL-2020-10025.

5. References

1. Ç. M. Oral, B. Ercan, *Powder Technol*. **2018,** *339,* 781–788. **DOI:**10.1016/j.powtec.2018.08.066
2. M. R. Abeywardena, R. K. W. H. M. K. Elkaduwe, D. G. G. P. Karunarathne, H. M. T. G. A. Pitawala, R. M. G.Rajapakse, A. Manipura, M. M. M. G. P. G. Mantilaka, *Adv. Powder Technol.* **2020,** *31,* 269–278. **DOI:**10.1016/j.apt.2019.10.018
3. H. Cölfen, *Curr. Opin. Colloid Interface Sci*. **2003,** *8,* 23–31. **DOI:**10.1016/S1359-0294(03)00012-8
4. J. D. Rodriguez-Blanco, S. Shaw, L. G. Benning, *Nanoscale.* **2011,** *3,* 265–271. **DOI:**10.1039/C0NR00589D
5. J. Zhang, S. Yuzhu, Y. Jianguo, *J. Cryst. Growth.* **2017,** *478,* 77–84.
6. H. Li, Q. Yao, F. Wang, Y. Huang, S. Fu, G. Zhou, *Geochim. Cosmochim. Acta.* **2019,** *256,* 35–48. **DOI:**10.1016/j.gca.2018.06.011
7. N. Erdogan, H. Ali Eken, *Physicochem. Probl. Miner. Process.* **2017,** *53,* 57–68.
8. T. Kato, A. Sugawara, N. Hosoda, *Adv. Mater.* **2002,** *14,* 869–877. **DOI:**10.1002/1521-4095(20020618)14:12<869::AID-ADMA869>3.0.CO;2-E
9. H. Saulat, M. Cao, M. M. Khan, M. Khan, K. Muhammad, M. M. Khan, A. Rehman, *Constr Build Mater.* **2020,** *236,* 117613. **DOI:**10.1016/j.conbuildmat.2019.117613
10. L. H. Fu, Y. Y. Dong, M. G. Ma, W. Yue, S. L. Sun, R. C. Sun, *Ultrason. Sonochem.* **2013,** *20,* 1188–1193. **DOI:**10.1016/j.ultsonch.2013.03.008
11. C. Carteret, A. Dandeu, S. Moussaoui, H. Muhr, B. Humbert, E. Plasari, *Cryst. Growth Des.* **2009,** *9,* 807–812. **DOI:**10.1021/cg800368u
12. M. Kitamura, *J. Cryst. Growth.* **2002,** *237,* 2205–2214. **DOI:**10.1016/S0022-0248(01)02277-1
13. E. MarieFlaten, M. Seiersten, *J. Crys Growth*. **2009,** *311,* 3533-3538. **DOI:**10.1016/j.jcrysgro.2009.04.014
14. Y. B. Hu, M. Wolthers, D. A. Wolf-Gladrow, G. Nehrke, *Cryst. Growth Des.* **2015,** *15,* 1596–1601. **DOI:**10.1021/cg500829p
15. W. S. Kim, I. Hirasawa, W. S. Kim, *Ind. Eng. Chem. Res.* **2004,** *43,* 2650–2657. **DOI:**10.1021/ie034161y
16. K. S. Raj, N. Devi, V.K. Subramanian, *Chem. Phys. Lett*. **2020,** *750,* 137502. **DOI:**10.1016/j.cplett.2020.137502
17. Q. Yao, Y. Wang, Y. Zhang, H. Li, G. Zhou, *Sci. China Earth Sci.* **2019,** *62,* 1619–1629. **DOI:**10.1007/s11430-018-9336-6
18. D. Zheng, H. Yang, F. Yu, B. Zhang, H. Cui, *Materials.* **2019,** *12,* 2045. **DOI:**10.3390/ma12132045
19. M. L. P. Vidallon, F. Yu, B.M. Teo, *Cryst. Growth Des.* **2020,** *20,* 645–652. **DOI:**10.1021/acs.cgd.9b01057
20. M. Kawanoa, T. Maeda, *J. Cryst. Growth.* **2020,** *535,* 125536. **DOI:**10.1016/j.jcrysgro.2020.125536
21. L. Stajner, J. Kontrec, B. N. Dzakula, N. Maltar-Strmecki, M. Plodinec, D. M. Lyons, D. Kralj, *J. Cryst. Growth.* **2018,** 486, 1–81. **DOI:**10.1016/j.jcrysgro.2018.01.023
22. A. W. Coats, J. Redfern, *Nature.* **1964,** *201,* 68–69. **DOI:**10.1038/201068a0
23. I. Mian, X. Li, Y. Jian, O. D. Dacres, M. Zhong, J. Liu, F. Ma, N. Rahman, *Bioresour. Technol.* **2019,** *294,* 122099. **DOI:**10.1016/j.biortech.2019.122099
24. S. R. Naqvi, R. Tariq, Z. Hameed, I. Ali, M. Naqvi, W. H. Chen, S. Ceylan, H. Rashid, J. Ahmad, S. A. Taqvi, M. Shahbaz, *Renew. Energy*. **2019,** *131,* 854-860. **DOI:**10.1016/j.renene.2018.07.094
25. Y. S. Kim, Y. S. Kim, S. H. Kim, *Environ. Sci. Technol.* **2010,** *44,* 5313–5317. **DOI:**10.1021/es101163e
26. K. M. Choi, K. Kuroda, *Cryst. Growth Des*. **2012,** *12,* 887–893. **DOI:**10.1021/cg201314k
27. Y. Liu, Y. Chen, X. Huang, G. Wu, *Mater. Sci. Eng. C.* **2017,** 79, 457–464. **DOI:**10.1016/j.msec.2017.05.085
28. N. L. Bolay, *Powder Technol.* **2003, 130,** 450-455. **DOI:**10.1016/S0032-5910(02)00249-8
29. S. Polat, *Adv. Powder Technol.* **2020,** *31,* 4282–4291. **DOI:**10.1016/j.apt.2020.09.003
30. A. Bastrzyk, M. Fiedot-Tobola, I. Polowczyk, K. Legawiec, G. Plaza, *Colloids Surf. B.* **2019,** *174,* 145–152. **DOI:**10.1016/j.colsurfb.2018.11.009
31. S. Kirboga, M. Oner, E. Akyol, *J. Cryst. Growth.* **2014,** *401,* 266–270. **DOI:**10.1016/j.jcrysgro.2013.11.048
32. S. Polat, *J. Cryst. Growth.* **2019,** *508,* 8–18. **DOI:**10.1016/j.jcrysgro.2018.12.017
33. M. A. Popescu, R. Isopescu, C. Matei, G. Fagarasan, V. Plesu, *Adv. Powder Techol.* **2014,** *25,* 500–507. **DOI:**10.1016/j.apt.2013.08.003
34. K. S. P. Karunadasa, C. H. Manoratne, H. M. T. G. A. Pitawala, R. M. G. Rajapakse,. *J. Phys. Chem. Solid.* **2019,** *134,* 21–28. **DOI:**10.1016/j.jpcs.2019.05.023
35. L. Fedunik-Hofman, A. Bayon, S.W. Donne, *Appl. Sci.* **2019,** *9,* 4601. **DOI:**10.3390/app9214601
36. L. Yue, M. Shui, Z. Xu, *Thermochim. Acta.* **1999,** *335,* 121–126. **DOI:**10.1016/S0040-6031(99)00174-4
37. Design-Expert software, Version 10 User's Guide, Stat-Ease.

Povzetek

Cilji predstavljene študije so bili sledeči: (i) določitev vpliva triptofana na transformacijo polimorfnih faz $CaCO_3$, (ii) preučitev kinetike in termodinamike toplotne razgradnje $CaCO_3$ s pomočjo Coats–Redfern-ove metode in (iii) določitev vpliva eksperimentalnih pogojev na delež vaterita pri $CaCO_3$ z metodologijo odzivnih površin in centralnega kompozitnega oblikovanja. Pripravljene kristale $CaCO_3$ smo analizirali z XRD, FTIR, SEM, BET, AFM in zeta potencialom. Rezultati karakterizacije so pokazali, da se oblika $CaCO_3$ kristalov spreminja od gladkih kockastih kristalov kalcita do nepravilnih, poroznih kristalov vaterita, z višanjem koncentracije triptofana. Kinetična študija termične razgradnje je pokazala, da krčenje sledi volumskemu delčnemu mehanizmu, R3, s povprečno aktivacijsko energijo 224.6 kJ/mol. Na osnovi rezultatov iz načrtovanje eksperimentov lahko zaključimo, da je koncentracija triptofana najpomembnejši dejavnik, ki vpliva na delež vaterita v pripravljenih kristalih. Triptofan torej omogoča boljše razumevanje in nadzor tvorbe polimorfov, velikosti in morfologije $CaCO_3$ kristalov.

Except when otherwise noted, articles in this journal are published under the terms and conditions of the Creative Commons Attribution 4.0 International License